Postsynaptic GluA1 enables acute retrograde enhancement of presynaptic function to coordinate adaptation to synaptic inactivity

Maria Lindskog, Li Li, Rachel D. Groth, Damon Poburko, Tara C. Thiagarajan, Xue Han, and Richard W. Tsien[1]

Department of Molecular and Cellular Physiology, Stanford University School of Medicine, Stanford, CA 94305

Prolonged blockade of AMPA-type glutamate receptors in hippocampal neuron cultures leads to homeostatic enhancements of pre- and postsynaptic function that appear correlated at individual synapses, suggesting some form of transsynaptic coordination. The respective modifications are important for overall synaptic strength but their interrelationship, dynamics, and molecular underpinnings are unclear. Here we demonstrate that adaptation begins postsynaptically but is ultimately communicated to presynaptic terminals and expressed as an accelerated turnover of synaptic vesicles. Critical postsynaptic modifications occur over hours, but enable retrograde communication within minutes once AMPA receptor (AMPAR) blockade is removed, causing elevation of both spontaneous and evoked vesicle fusion. The retrograde signaling does not require spiking activity and can be interrupted by NBQX, philanthotoxin, postsynaptic BAPTA, or external sequestration of BDNF, consistent with the acute release of retrograde messenger, triggered by postsynaptic Ca^{2+} elevation via Ca^{2+}-permeable AMPARs.

homeostasis | synaptic scaling | calcium signaling | miniature excitatory postsynaptic currents

Prolonged perturbations in the level of activity of neuronal circuits initiate major changes in excitatory transmission. Such retuning is generally homeostatic and is proposed to counterbalance other forms of plasticity and to help keep neuronal firing rate within an optimal range for efficient transfer of information (1–3). There is growing agreement about the functional significance of adaptation to inactivity (2, 4), but much uncertainty remains about where and how such adaptation is expressed.

The increase in postsynaptic function in response to prolonged inactivity, evident as an increase in the amplitude of unitary synaptic events (miniature excitatory postsynaptic currents, mEPSCs, or minis), is by now well-established (2, 4). The enlargement of mEPSCs is mediated by an accumulation of AMPA receptors (AMPARs) at postsynaptic sites (5–8). Sometimes the increase is attributed to an increase in Ca^{2+}-permeable AMPARs that lack GluA2 subunits (7, 9, 10), but in other cases comparable elevations in both GluA1 and GluA2 have been seen (6, 8, 11, 12). Furthermore, adaptation to inactivity induced by postsynaptic blockade may also involve presynaptic changes, reflected by an elevated frequency of mEPSCs and increased vesicular turnover (7, 13–16).

Although evidence is mounting for both pre- and postsynaptic modifications, the fundamental nature of such alterations remains incompletely understood. On one hand, neuronal inactivity causing cellwide changes in transmitter release and receptivity (2) would fit with descriptions of synaptic homeostasis as a global phenomena. This idea is supported by evidence showing that glial cells can serve as general activity sensors and modulate all synapses in an area (17). On the other hand, findings of tight coordination between closely neighboring synapses (18) and of differential regulation of different types of synapses (19) would be compatible with a synapse-based organization.

Transsynaptic coordination is of general interest because the efficacies of pre- and postsynaptic components are multiplicative factors, making concerted increases all the more powerful (7, 20–22). In principle, coordination could arise from a physical linkage of pre- and postsynaptic elements (discussed in ref. 13) or from a primary up-regulation on one side that drives secondary changes on the other (11, 23, 24).

Additional uncertainty exists regarding the time scale of adaptive changes. At the fly neuromuscular junction (NMJ), adaptation to inactivity depends critically on acute changes in physiological function (25–27). In striking contrast, signaling at synapses between mammalian CNS neurons is thought to proceed over several hours (10, 28) if not days (1, 7).

We have studied homeostatic adaptation at synapses between cultured hippocampal neurons with a combination of electrophysiology, immunocytochemistry, and dynamic imaging. The adaptation to inactivity includes a postsynaptically induced up-regulation of presynaptic function in both spontaneous and evoked release. This form of homeostatic plasticity could provide a form of rapid, coordinated enhancement on both sides of the synapse that yields a greater efficiency of neurotransmission.

Results

Increased Presynaptic Activity: An Acute Effect Requiring AMPA Receptor Activation. In our previous work where we showed increased pre- and postsynaptic efficacy (7), it remained unclear (29) whether the modification of presynaptic properties developed entirely during the inactivity period or was triggered in part by the relief of inactivity (30). To distinguish between these scenarios, presynaptic activity was assessed both during and following the relief of activity blockade. We first used the uptake of an antibody that binds to a luminal epitope of synaptotagmin (Syt-Ab) (Fig. 1), which is taken up by synaptic vesicles when they release neurotransmitter (31, 32). Excitatory synaptic activity was blocked for 24 h by inhibiting AMPA receptors with 10 µM of NBQX in the culture medium. As a control, we used sister cells from the same cultures without the 24-h activity deprivation. After washout of NBQX, cells were allowed to take up the Syt-Ab for 5 min in the presence of TTX and bicuculline, then fixed and counterstained for synapsin to identify synapses (Fig. 1A). To focus on changes in vesicle turnover, we chose regions of interest where synapsin staining was not different. For each condition, we determined the synapsin-IR and the Syt-Ab uptake from 50 to 200 synapsin positive puncta per area in 16–20 areas from at least four different experiments. All values for Syt-Ab

Fig. 1. Increased presynaptic activity is a sustained effect dependent on active AMPA receptors. (A) Uptake of Syt-Ab (green) in the presence of TTX + bicuculline over 5-min periods, in untreated cells (control) and in cells treated with NBQX for 24 h, beginning at 5, 30, and 240 min after washout of NBQX. Immunostaining for synapsin (red) provided a synaptic marker. (B) Average Syt-Ab uptake per synapse (synapses defined by synapsin staining), normalized to Syt-Ab uptake in non-NBQX–treated cells. Syt-Ab uptake is significantly increased 5 and 30 min after washout of NBQX (filled symbols), but not in control experiments when NBQX remains continuously present after a sham washout (open symbols). *$P < 0.01$ (ANOVA) for cells subjected to NBQX removal compared with mock washout at same time point.
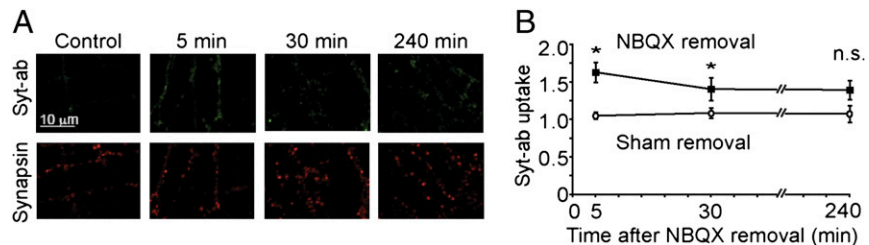
uptake were normalized to the average Syt-Ab uptake in control cells. As we have previously reported, 24-h treatment of NBQX led to an increase in average Syt-Ab uptake (1.60 ± 0.15 of control at 5 min after NBQX washout, $n = 3587$, $P < 0.005$) (Fig. 1B). In contrast, Syt-Ab uptake was not significantly increased (1.02 ± 0.05) 5 min after the sham washout procedure. Thus, the increase in presynaptic activity observed after prolonged NBQX treatment was dependent on restoration of AMPAR functionality.

To determine whether the presynaptic response was a transient modification, consistent with a simple rebound phenomenon, or a sustained enhancement, we monitored the presynaptic activity after increasing NBQX washout time. The 24-h treatment of NBQX led to an increase in Syt-Ab uptake that was persistent beyond the immediate effect: 1.37 ± 0.10 of control at 30 min ($n = 4271$, $P < 0.01$), and 1.39 ± 0.20 of control at 240 min ($n = 4064$, $P < 0.06$) (Fig. 1B). In contrast, Syt-Ab uptake was not significantly increased at any time point (1.06 ± 0.06 and 1.05 ± 0.10 of control after 30 and 240 min, respectively) after the sham solution exchange (NBQX continuously present). Using the data from the sham washout condition as a basis of comparison, the genuine washout produced a significant increase in Syt-Ab uptake 5 and 30 min after washout ($P < 0.01$, ANOVA).

In a control experiment, we showed that blockade of AMPA receptors during a 4-h Syt-Ab uptake procedure did not have any effect in cells that had not previously been treated with NBQX (0.96 ± 0.04 of control). Thus, AMPAR blockade generated an increase in presynaptic activity that was critically dependent on the removal of the blockade, did not require spiking activity during the removal, and lasted for at least 0.5 h.

NMDAR Minis Monitor Unitary Synaptic Activity and Verify an Acute Presynaptic Enhancement. To confirm the increase in vesicular turnover, we turned to miniature EPSCs generated by postsynaptic NMDA receptors (33). We chose recording conditions that favor NMDA currents (10 μM glycine, no Mg^{2+}, and elevated extracellular Ca^2), and used template-based detection (34) (Fig. S1). Under control conditions, the frequency of detected minis was the same whether or not the AMPARs were blocked (Fig. S2), indicating that the NMDAR mini detection had a sensitivity for presynaptic release comparable to that of conventional minis. This conclusion was corroborated by close agreement of the amplitude of NMDA-only minis and the amplitude of the slowly decaying tail (NMDA component) of minis detected by their AMPA component (Fig. S2B); the NMDA-only events showed no detection bias toward large events as would be expected if there had been substantial loss of small events in the noise.

Accordingly, we used NMDA minis to study possible presynaptic changes following the cessation of a prolonged blockade of AMPARs (Fig. 2). The baseline frequency of NMDA minis in the continuous presence of NBQX averaged 0.87 ± 0.12 Hz ($n = 7$) (Fig. 2A). Doing a sham solution exchange that left the AMPAR blocked by NBQX did not significantly change the

frequency (0.55 ± 0.10 Hz, $n = 3$, $P > 0.09$). In contrast, when NBQX was removed, the mini frequency rose to 1.31 ± 0.13 Hz ($P < 0.05$, $n = 4$). The increase was also significant compared with baseline levels in the cells where NBQX was later washed out ($P < 0.03$, $n = 4$). The electrophysiological measurements of neurotransmission corroborated the immunocytochemical assays
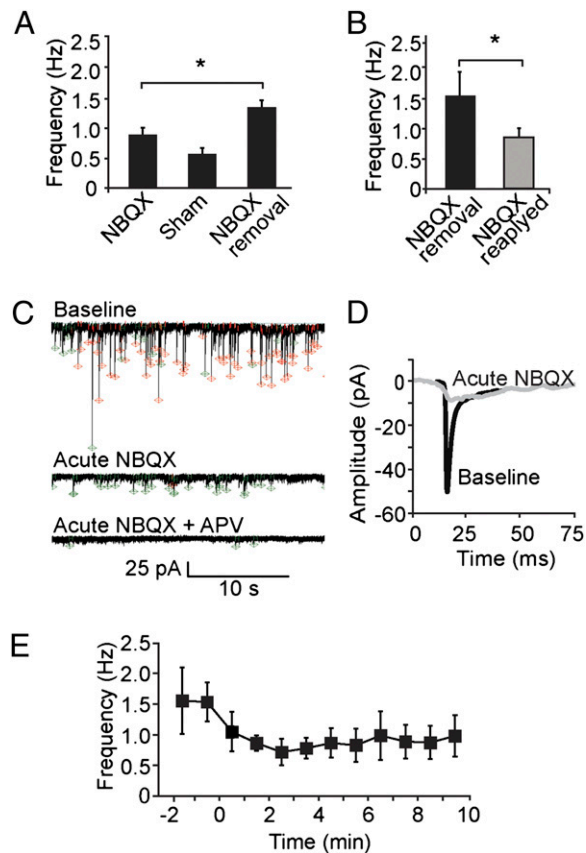

Fig. 2. Increased frequency of NMDA minis following cessation of AMPAR blockade is reversed upon reapplication of AMPAR blocker. (A) Average frequency of mEPSC events in 24-h NBQX-treated neurons is increased upon removal of NBQX ($P < 0.05$), but not in sham removal control. (B) Reapplication of NBQX causes mini frequency increase to subside (return to baseline depicted in Fig. 2A). (C) Representative traces (1 min) illustrating effect of NBQX reexposure and of further exposure to APV. Events detected using NMDA and mixed mini templates marked in green and red, respectively. (D) Averaged events for baseline (black) and after acute NBQX reapplication (gray) exhibit a decreased AMPA component without any loss of NMDA component (for interpretation, see text). (E) Time course of reduction in mini frequency (1-min averages) caused by reapplication of NBQX (at time 0) to neurons previously subjected to 24-h NBQX treatment and ~20-min washout before start of recording.

(Fig. 1). In the wake of prolonged AMPA receptor blockade, restoration of AMPAR activity produced an elevation in presynaptic activity within minutes.

Reapplication of NBQX Rapidly Suppresses Increased Presynaptic Activity. To determine whether the increased presynaptic activity could be reversed, we examined the effects of NBQX reapplication. Roughly 20 min following washout of NBQX (prior 24-h treatment), whole cell recordings were begun with both AMPA and NMDA receptors active. In previously transmission-blocked cells, reblock of AMPA receptors (NBQX, 10 μM) reduced the frequency of spontaneous transmission (whether detected as mixed events or purely NMDAR minis) (Fig. 2) from 1.54 ± 0.42 Hz to 0.83 ± 0.20 Hz ($P < 0.05$, t test, $n = 4$) (Fig. 2B). This contrasted with the lack of change in mini frequency observed in control cells upon NBQX application (Fig. S2C). Acute NBQX eliminated the fast AMPA component but did not enlarge the slow NMDA component (Fig. 2D). This indicated that large events were not overrepresented, as would be expected if NMDA-only minis had been less efficiently detected than minis including AMPAR current.

The time course on a minute-by-minute basis (Fig. 2E) emphasizes that in previously transmission-deprived cells, reblocking AMPA receptors leads to an acute decrease in mini frequency. The decrease was already significant during the second minute after beginning the NBQX perfusion and was much more rapid (minutes) than the initial events in the development of adaptation to inactivity (hours) (see ref. 35).
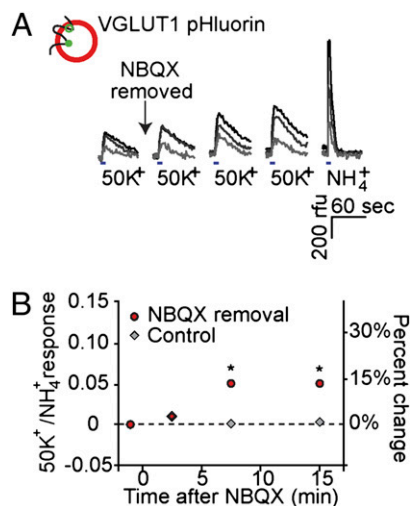

Fig. 3. Effect of NBQX removal on depolarization-evoked synaptic vesicle turnover. (A) Examples of VGLUT1–pHluorin fluorescence responses in single boutons exposed to 50 mM K^+ and 50 mM NH_4^+. Three representative single boutons were chosen from the NBQX-treated coverslip that gave the median response to 24-h NBQX treatment to illustrate progressive increases in high K^+ responses following NBQX removal. Four second long K^+ challenges were administered ∼1 min before, and 2.5, 7.5, and 15 min after removal of NBQX. Response amplitudes at the end of the K^+ challenge were used for further analysis. Subsequent NH_4^+ responses (3-s exposure) provide a gauge of the fluorescently labeled vesicle pool in the same three boutons and illustrate a typical range of amplitudes. (B) Pooled data showing progressive enhancement of depolarization-dependent VGLUT1–pHluorin fluorescence signals following NBQX washout. Change in the relative size of the synaptic responses evoked by 50 mM K^+, referenced to a subsequent response to NH_4^+ in the same bouton (*Left* vertical axis). Data points and error bars show mean ± SEM of individual bouton responses (error bars not seen when within the size of the symbols). *Right* vertical axis shows the fractional increase referenced to basal ratio. *$P < 0.001$ for comparison between NBQX removal and control at a given time point.

Increase in Evoked Transmission Following Cessation of AMPAR Blockade. Given that spontaneous minis and evoked release may not arise from the same pool of synaptic vesicles (33, 36, 37), we wanted to know whether evoked release was also increased after blocking of synaptic transmission. Here we monitor vesicle turnover by measuring the fluorescence increase of VGLUT1–pHluorin (38) when the interior of the acidified vesicle comes in contact with the pH neutral external medium. This method also has the advantage of working equally well regardless of the mode of release (i.e., full collapse versus kiss and run), whereas Syt-Ab uptake may depend on the mode of release. Hippocampal cultures were exposed to NBQX for 24 h. Assays were performed in NBQX-free solution (or NBQX-containing solution in case of sham washout) in the presence of TTX, and exocytosis was triggered by local application of a solution containing 50 mM K^+, thereby bypassing any confounding changes in excitability or action potential shape (Fig. 3). Exocytotic responses were evoked before and 2.5, 7.5, and 15 min after the removal of NBQX. As a measure of the total population of fluorescently labeled synaptic vesicles, the last K^+ depolarization was followed by an application of ammonium chloride, to produce vesicle deacidification without exocytosis (Fig. 3A).

Following the termination of AMPAR block, the evoked responses grew progressively larger, both in rising slope and peak magnitude. The synaptic vesicle pool was not exhausted by any of the K^+ challenges; K^+ responses are smaller than responses evoked by an NH_4Cl challenge in the same boutons (Fig. 3A). Fig. 3B presents pooled data for a large number of boutons ($n = 939$, $n = 8$), displayed as a percent change in the ratio of amplitudes of the K^+ and NH_4^+ responses. The NH_4^+ response provided an index of cumulative release probability, with each nerve terminal serving as its own reference. The fractional change over the course of 10–15 min was ∼15%. In the control experiments, K^+-induced responses remained unchanged after the sham NBQX removal (Fig. 3B; $n = 1,085$, $n = 9$). The data for NBQX removal and for control showed significant differences at the 7.5- and 15-min time points, ($P < 0.001$). There was no difference in the proportion of active synapses in control cells versus cells that had been treated with NBQX for 24 h (Fig. S3). Thus, VGLUT1–pHluorin experiments provided a third line of evidence that presynaptic activity was acutely enhanced after termination of chronic NBQX block and also demonstrated that the enhancement extends to evoked release.

The Presynaptic Enhancement Is Dependent on Active GluA1 Homomers. We hypothesized that the increase in presynaptic activity is mediated by GluA1 homomers that are up-regulated
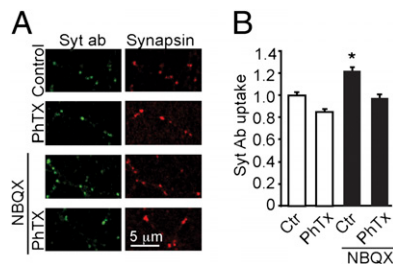

Fig. 4. GluA1 homomers mediate the increase in presynaptic activity. (A) Transmission-deprived cells, as well as control cells, were allowed to take up Syt-Ab (green) for 4 h in the absence or presence of PhTx under conditions where network activity was blocked (TTX + bicuculline). The cells were then fixed and stained for synapsin (red) as a synaptic marker. (B) Average Syt-Ab uptake per synapse. When PhTX is present during the antibody uptake, the amount of antibody taken up is not different from control levels. When NBQX is washed out, Syt-Ab uptake is significantly increased compared with all other groups ($P < 0.01$, ANOVA); thus the presence of PhTx during the uptake prevented the increase in Syt-Ab following 24 h of transmission blockade.

during the period of activity blockade. To test this hypothesis we used philanthotoxin (PhTx) as a selective blocker of GluA1 homomers (Fig. 4). In each condition, Syt-Ab uptake was measured in >400 synapses in 12–16 areas of analysis and average normalized Syt-Ab uptake for each condition is shown. The presence of PhTx during Syt-Ab uptake in control (nonactivity deprived) cells did not cause a significant decrease in Syt-Ab intensity (0.85 ± 0.05 of control). In contrast, 24-h NBQX treatment increased Syt-Ab uptake to 1.22 ± 0.11 of control ($P < 0.02$). In the presence of PhTx (10 µM), the inactivity-induced increase was no longer observed; the levels of Syt-Ab uptake fell close to control ($97 \pm 3\%$ of control). There was no significant difference in the synapsin staining in any of the conditions. These results indicated that GluA1 homomers play a causal role in linking inactivity to enhancement of presynaptic vesicular turnover.

Testing for Retrograde Signaling by Cell-Autonomous Intervention.
The results thus far do not distinguish between changes originating in the postsynaptic cell, generating a retrograde signal, and those initiated acutely within the presynaptic neuron. The observation that blocking GluA1 homomers reverses the increase in mini frequency raises the possibility that the Ca^{2+} influx is the signal that initiates retrograde communication. Accordingly, we tested for involvement of a change in postsynaptic Ca^{2+} level by introducing BAPTA (10 mM) into the postsynaptic cell via the recording pipette (Fig. 5). Whereas mini frequency was significantly elevated in neurons relieved from chronic NBQX treatment as compared with those in basal conditions, 6.7 ± 1.0 Hz ($n = 18$) versus 3.3 ± 0.8 Hz ($n = 7$, $P < 0.03$), no such elevation was observed when postsynaptic Ca^{2+} was buffered with internal BAPTA (3.5 ± 0.7 Hz, $n = 14$, $P > 0.4$). In neurons that had not been subjected to prolonged block of AMPARs, inclusion of internal BAPTA did not cause a significant difference in mini frequency ($P > 0.25$). These results verify that presynaptic changes in exocytosis are specifically initiated in the postsynaptic neuron and support the idea that a rise in intracellular Ca^{2+} level, mediated by Ca^{2+}-permeable glutamate receptors, triggers the retrograde signal.
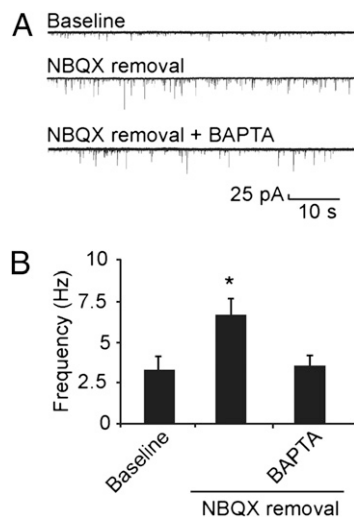
Fig. 5. Postsynaptic BAPTA prevents mini frequency increase after removal of transmission blockade. (*A*) Representative 1-min recordings of conventional minis from hippocampal neurons in control, NBQX washout, and BAPTA + NBQX washout conditions. (*B*) Pooled data for the same three categories, showing that the presence of postsynaptic BAPTA (10 mM in pipette) prevented the mini frequency increase upon relief from chronic NBQX treatment ($P > 0.4$ relative to control).
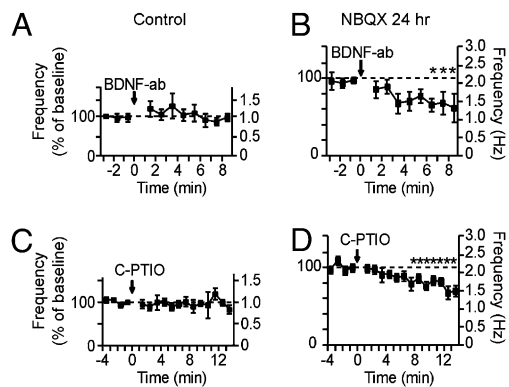
Fig. 6. BDNF antibody and NO scavenger decrease mini frequency in transmission-deprived cells. (*A* and *B*) Effect of exposure to a BDNF-neutralizing antibody (BDNF-Ab) to inactivate released BDNF. This treatment has no effect on mini frequency in control cells (*A*), but significantly decreases mini frequency in transmission-deprived cells (*B*). (*C* and *D*) Effect of exposure to a NO-scavenging agent, carboxy-PTIO (C-PTIO). After 4 min of baseline mEPSC recordings, cells were exposed to C-PTIO to prevent extracellular NO signaling. C-PTIO did not affect mini frequency in control cells (*C*), but slowly reduced it in transmission-deprived cells (*D*). Data shown as average mini frequency (1/interval) per minute, normalized to baseline frequency for each cell. *Right* axes represent the corresponding average frequency. For activity-deprived cells, *y* axes have been scaled to reflect the average increase in frequency due to transmission deprivation compared with control. Error bars denote SEM; *$P < 0.05$, t test, average mini frequency per minute, compared with average baseline frequency.

Evaluating Candidates for Conveying a Retrograde Signal. The BAPTA experiments establish the existence of retrograde communication from post to pre but leave open the identity of the retrograde messenger(s). Among multiple candidates BDNF and NO emerged as the most promising (*SI Text*). We used a BDNF antibody (BDNF-Ab, 100 ng/mL) that selectively binds and inactivates released BDNF (39). Acute application of the BDNF-Ab did not significantly change mini frequency in control cells (1.12 ± 0.19 of baseline frequency, $P > 0.8$, t test, $n = 5$) (Fig. 6*A*). In contrast, in activity-deprived neurons, exposure to BDNF-Ab caused a decrease in mini frequency (0.69 ± 0.24 of baseline, $P < 0.01$, t test, $n = 6$) (Fig. 6*B*). After scaling of the vertical axis to reflect the average increase in basal frequency after transmission deprivation (1.80 ± 0.28-fold greater than control), this plot shows that the BDNF scavenger brought the mini frequency back down to a level close to control ($P > 0.5$ from $t = 6$ min onwards).

The possible role of NO was assessed using carboxy-PTIO (C-PTIO), a powerful scavenger that binds and inactivates NO (40). Although C-PTIO did not exert any effect on mini frequency in control cells (0.96 ± 0.04 of baseline frequency, $n = 10$, $P > 0.7$, t test) (Fig. 6*C*), it significantly decreased mini frequency in activity-deprived cells (0.84 ± 0.03 of baseline frequency 5 min after C-PTIO application, $P < 0.03$, t test, $n = 9$) (Fig. 6*D*). After allowing for the increase in baseline mini frequency in the transmission-deprived cells (1.82 ± 0.33-fold greater than control cells), it appeared that C-PTIO caused a partial reversion of the net increase induced by removal of AMPAR block. This raised the possibility that BDNF and NO might work in parallel, but we also considered the idea that NO and BDNF act in series, along an extended signaling pathway. The possibility of parallel action was tested by concomitantly blocking both messengers. The effect of applying both BDNF-Ab and C-PTIO was significant (0.76 ± 0.06 of baseline frequency, $n = 7$, $P < 0.01$, t test), and larger than that of C-PTIO alone ($P < 0.03$, t test), but not greater than that obtained with BDNF-Ab on its own ($P > 0.5$, t test). The occlusion

of the effect of C-PTIO by BDNF-Ab was consistent with the hypothesis that NO and BDNF operate in series.

Discussion

We focused on a form of synaptic adaptation to reduced activity that features enhancements of synaptic function on both sides of the synapse. Our experiments show that blockade of fast neurotransmission for 24 h sets the stage for acute retrograde signaling once the AMPAR blocker is withdrawn. During the period of inactivity, the prevalence of postsynaptic, Ca^{2+}-permeable GluA1-containing receptors is increased. Then, relief of blockade allows Ca^{2+} permeation through GluA1 homomers, triggering rapid, Ca^{2+}-dependent signaling back to the presynaptic terminal to elevate release probability. Thus, adaptation to inactivity not only requires molecular events that emerge over the course of hours, but also recruits rapid, retrograde signaling that takes place within minutes after activity is restored.

Role of Rapid AMPAR-Dependent Retrograde Signaling to Presynaptic Terminals.

We used three different methods to monitor presynaptic activity that bypass AMPARs: measuring Syt-Ab uptake (Figs. 1 and 4), recording unitary transmission via NMDARs (Fig. 2) and imaging VGLUT1–pHluorin (Fig. 3). In this way, we were able to demonstrate significant increases in presynaptic function following removal of chronic postsynaptic AMPA receptor blockade (Figs. 1–4), and reversal of such increases upon reassertion of such blockade (Figs. 2 and 4). In both situations, changes were apparent within ~5–10 min. The recordings of NMDAR minis provided the best temporal resolution of the kinetics of these changes, whereas Syt-Ab uptake and VGLUT1–pHluorin signals provided the most rigorous evidence for its presynaptic nature. Our experiments focused on determining the importance of retrograde signaling to modify presynaptic function and did not address questions of whether excitability of nerve terminals is altered (41), or whether presynaptic excitability gates the outcome of chronic AMPAR blockade, as reported by Jakawich et al. (35).

Evaluating the Candidate Retrograde Messengers BDNF and NO.

Scavenging of extracellular BDNF reduced the mini frequency increase in activity-deprived neurons within 5 min, but left mini frequency in control recordings unchanged (Fig. 6). Participation of BDNF would be consistent with its ability to rapidly increase mini frequency in hippocampal cultures (42, 43) and with the effects of postsynaptic BDNF knockdown (35). In contrast, the effect of C-PTIO was slow to develop (Fig. 6), even though it is a small molecule that should reach the synaptic cleft at least as quickly as BDNF-Ab. When we presented BDNF-Ab and C-PTIO in combination, we found no increase in the degree of suppression of mini frequency, weighing against the idea that NO acts completely independently of BDNF. NO is known to act by increasing cGMP to activate cGMP-dependent protein kinase, leading to externalization of GluA1 (44). According to this scenario, C-PTIO would act as a sink for intradendritic NO, which may favor a net internalization of GluA1 and thereby slowly dampen GluA1-dependent signaling, including Ca^{2+}-triggered release of BDNF.

Basis of Transsynaptic Coordination.

Coordination between pre- and postsynaptic determinants of synaptic strength is featured in both theoretical approaches (22, 45) and experimental studies of cortical networks (46, 47). We have previously reported correlations between increases in presynaptic P_r and postsynaptic GluA1 (7) but the mechanistic basis of such coordination is unclear. A physical yoking together of pre- and postsynaptic components may occur, but we propose that in addition there exists an acute signal from the postsynaptic side that modifies physiological properties on the presynaptic side. Precedent for rapid retrograde transmission, occurring over the course of minutes, can be found at the neuromuscular junction in *Drosophila* (25).

It has previously been shown that spontaneous vesicle release (minis) can drive the slow synaptic changes that take place during homeostatic plasticity (10, 25, 48). Our NBQX washout experiments were done in the presence of TTX, suggesting that spontaneous vesicle release is also sufficient to trigger acute retrograde signaling over the course of minutes. The finding of evidence for retrograde communication does not exclude the additional possibility of orthograde signaling as a further mechanism of transsynaptic coordination. Orthograde signaling has been invoked to explain how presynaptic activity regulates the gathering together of GluA1 (11, 24, 49). Full coordination might require a combination of signaling in both directions.

Methods

Cell Culture. CA3–CA1 hippocampal neurons were cultured as previously described (50). Cells were deprived of synaptic activity for 24 h by adding 10 μM of NBQX to culture wells after 14–16 d in vitro (DIV).

Syt-Ab Uptake. Cells that had been treated with NBQX for 24 h, or control cells from the same culture, were transferred to Tyrode solution (150 m NaCl, 4 mM KCl, 2 mM MgCl2, 2 mM CaCl2, 10 mM Hepes, 10 mM glucose, osmolarity 310 mOsm) containing TTX (1 μM), bicuculline (5 μM) and the antibody against the luminal epitope of synaptotagmin (Synaptic Systems, 105221, 1:100), plus NBQX (10 μM) or philanthotoxin (10 μM) as indicated. Cells were incubated with the Syt-Ab at 37 °C for either 5 min (Fig. 1) or 4 h (Fig. 4) and then washed in ice-cold PBS and fixed in 4% paraformaldehyde containing 10 mM EGTA and 4% sucrose for 10 min. After blocking in 10% goat serum for 30 min, and then permeabilization in 0.1% Triton X-100, cells were incubated overnight with synapsin antibody (Synaptic Systems), washed, and incubated with fluorescently tagged secondary antibodies for 1 h. Cells were mounted in antifading mounting medium (Vectashield or Fluoromount) for subsequent imaging and analysis.

When studying NBQX washout, the cells were superfused with Tyrode solution for 2 min to wash out NBQX after the 24-h treatment and then immersed in conditioned culture medium without NBQX for the rest of the washout period (3, 28, and 238 min, respectively). After the washout period, cells were transferred to Tyrode solution containing TTX (1 μM) bicuculline (5 μM), and an antibody against the luminal epitope of synaptotagmin (Synaptic Systems, 105221, 1:100). Cells from the same culture that had not been subjected to 24-h NBQX treatment were used as controls.

Images were acquired on a Zeiss LSM 510 confocal laser scanning microscope in one confocal plane, pinhole 1 AU, using consecutive scanning in two channels for synapsin and synaptotagmin, respectively. Images were analyzed with ImageJ software (http://rsbweb.nih.gov/ij/). Regions of interest (ROIs) were identified as synapsin-positive puncta that were between 0.05 and 4 μm² in area. The ROIs were overlaid on the channel showing the Syt-Ab uptake, and the amount of fluorescence within each ROI was measured. The Syt-Ab labeling at each synapse was normalized to the average Syt-Ab labeling under control conditions before averaging.

Assay of Evoked Vesicle Fusion with VGLUT1–pHluorin. Cells were imaged at 14–17 DIV and treated with NBQX (10 μM) 22–26 h before imaging. Cells were superfused for 10 min at 1.5 mL/min with Tyrode solution (see above) containing NBQX (10 μM), TTX (1 μM), APV (10 μM), and bicuculline (10 μM). A field of view was selected on the basis of VAMP2–mCherry expression and morphology, and VGLUT1–pHluorin coexpression was confirmed by locally superfusing cells with a pulse of NH4Cl (50 mM). Synaptic vesicle fusion was evoked by pulse-like, local application of Tyrode containing 50 mM K⁺ (equimolar replacement of NaCl by KCl). Subsequently, the superfusion solution was switched to NBQX-free Tyrode still containing TTX, APV, and bicuculline, and three additional K⁺ challenges were imposed. Ten minutes after the fourth 50-mM K⁺ challenge, cells were exposed to NH4⁺ to assess total vesicle pool size. Images were acquired at 2 Hz for 10 s before stimuli, at 4 Hz during stimuli, and at 0.5 Hz for 60 s during recovery. Boutons were automatically detected in ImageJ (v1.43o, http://rsbweb.nih.gov/ij/) on the basis of NH4⁺ responses from VGLUT1–pHluorin. Experiments were performed at ambient temperature (22–23 °C).

Electrophysiology. Neurons at 16–20 DIV were held under voltage clamp at –60 mV and mEPSCs were recorded in a bath extracellular Tyrode solution at ambient temperature (150 mM NaCl, 4 mM KCl, 2 mM MgCl2, 2 mM CaCl2, 10 mM Hepes, 10 mM glucose, osmolarity 310 mOsm): intracellular solution 135 mM CsMeSO4, 5 mM KCl, 4 mM MgCl2, 1 mM EGTA, 9 mM

Hepes, 5 mM ATP, osmolarity 295 mOsm) containing 1 μM TTX and 10 μM bicuculline. Series resistance was left uncompensated. Only cells with series resistance between 10 and 20 MΩ that did not change more than 20% during the recording were used in the comparisons of mEPSC properties. Conventional mEPSCs were analyzed using Synaptosoft software. The threshold for detection was set at 7 pA and cells with noisy baselines were not used in the analysis. NMDA minis were recorded using the same intra- and extracellular solutions, but with extracellular magnesium removed and Ca^{2+} increased to 3 mM and in the presence of 10 μM glycine to optimize NMDA detection. For NMDA mini analysis, see *SI Text*.

Acute perfusion of PhTx (10 μM), NBQX (10 μM), anti-BDNF antibody (100 ng/mL; Calbiochem) or carboxy-PTIO (30 μM) was carried out for at least 6 min after ≥3 min of baseline recording.

BAPTA experiments were conducted using the above intracellular solution containing either 0.4 mM EGTA or 10 mM BAPTA replacing the EGTA. A 10-min perfusion at >1.5 mL/min was used to wash out NBQX from chronically treated cells. Only recordings after the 10-min washout were used for analysis.

Statistics. Unless otherwise noted, data are shown as mean value ± SEM and compared using Student's *t* test (if only two groups) or ANOVA followed by a Bonferroni posttest for multiple groups (if more than two groups were compared).

1. Turrigiano GG, Leslie KR, Desai NS, Rutherford LC, Nelson SB (1998) Activity-dependent scaling of quantal amplitude in neocortical neurons. *Nature* 391:892–896.
2. Turrigiano G (2007) Homeostatic signaling: The positive side of negative feedback. *Curr Opin Neurobiol* 17:318–324.
3. Burrone J, Murthy VN (2003) Synaptic gain control and homeostasis. *Curr Opin Neurobiol* 13:560–567.
4. Davis GW (2006) Homeostatic control of neural activity: From phenomenology to molecular design. *Annu Rev Neurosci* 29:307–323.
5. Liu G, Tsien RW (1995) Properties of synaptic transmission at single hippocampal synaptic boutons. *Nature* 375:404–408.
6. O'Brien RJ, et al. (1998) Activity-dependent modulation of synaptic AMPA receptor accumulation. *Neuron* 21:1067–1078.
7. Thiagarajan TC, Lindskog M, Tsien RW (2005) Adaptation to synaptic inactivity in hippocampal neurons. *Neuron* 47:725–737.
8. Wierenga CJ, Ibata K, Turrigiano GG (2005) Postsynaptic expression of homeostatic plasticity at neocortical synapses. *J Neurosci* 25:2895–2905.
9. Ju W, et al. (2004) Activity-dependent regulation of dendritic synthesis and trafficking of AMPA receptors. *Nat Neurosci* 7:244–253.
10. Sutton MA, et al. (2006) Miniature neurotransmission stabilizes synaptic function via tonic suppression of local dendritic protein synthesis. *Cell* 125:785–799.
11. Hou Q, Zhang D, Jarzylo L, Huganir RL, Man HY (2008) Homeostatic regulation of AMPA receptor expression at single hippocampal synapses. *Proc Natl Acad Sci USA* 105:775–780.
12. Cingolani LA, et al. (2008) Activity-dependent regulation of synaptic AMPA receptor composition and abundance by beta3 integrins. *Neuron* 58:749–762.
13. Murthy VN, Schikorski T, Stevens CF, Zhu Y (2001) Inactivity produces increases in neurotransmitter release and synapse size. *Neuron* 32:673–682.
14. Bacci A, et al. (2001) Chronic blockade of glutamate receptors enhances presynaptic release and downregulates the interaction between synaptophysin-synaptobrevin-vesicle-associated membrane protein 2. *J Neurosci* 21:6588–6596.
15. Thiagarajan TC, Piedras-Renteria ES, Tsien RW (2002) alpha- and betaCaMKII. Inverse regulation by neuronal activity and opposing effects on synaptic strength. *Neuron* 36:1103–1114.
16. Gong B, Wang H, Gu S, Heximer SP, Zhuo M (2007) Genetic evidence for the requirement of adenylyl cyclase 1 in synaptic scaling of forebrain cortical neurons. *Eur J Neurosci* 26:275–288.
17. Stellwagen D, Malenka RC (2006) Synaptic scaling mediated by glial TNF-alpha. *Nature* 440:1054–1059.
18. Branco T, Staras K, Darcy KJ, Goda Y (2008) Local dendritic activity sets release probability at hippocampal synapses. *Neuron* 59:475–485.
19. Kim J, Tsien RW (2008) Synapse-specific adaptations to inactivity in hippocampal circuits achieve homeostatic gain control while dampening network reverberation. *Neuron* 58:925–937.
20. Sejnowski TJ (1977) Statistical constraints on synaptic plasticity. *J Theor Biol* 69:385–389.
21. Montague PR, Sejnowski TJ (1994) The predictive brain: Temporal coincidence and temporal order in synaptic learning mechanisms. *Learn Mem* 1:1–33.
22. Buonomano DV (2005) A learning rule for the emergence of stable dynamics and timing in recurrent networks. *J Neurophysiol* 94:2275–2283.
23. Burrone J, O'Byrne M, Murthy VN (2002) Multiple forms of synaptic plasticity triggered by selective suppression of activity in individual neurons. *Nature* 420:414–418.
24. Harms KJ, Tovar KR, Craig AM (2005) Synapse-specific regulation of AMPA receptor subunit composition by activity. *J Neurosci* 25:6379–6388.
25. Frank CA, Kennedy MJ, Goold CP, Marek KW, Davis GW (2006) Mechanisms underlying the rapid induction and sustained expression of synaptic homeostasis. *Neuron* 52:663–677.
26. Petersen SA, Fetter RD, Noordermeer JN, Goodman CS, DiAntonio A (1997) Genetic analysis of glutamate receptors in Drosophila reveals a retrograde signal regulating presynaptic transmitter release. *Neuron* 19:1237–1248.
27. Paradis S, Sweeney ST, Davis GW (2001) Homeostatic control of presynaptic release is triggered by postsynaptic membrane depolarization. *Neuron* 30:737–749.
28. Ibata K, Sun Q, Turrigiano GG (2008) Rapid synaptic scaling induced by changes in postsynaptic firing. *Neuron* 57:819–826.
29. Gundlfinger A, Schmitz D (2005) Inactivity sets XL synapses in motion. *Neuron* 47:623–625.
30. Sokolova IV, Mody I (2008) Silencing-induced metaplasticity in hippocampal cultured neurons. *J Neurophysiol* 100:690–697.
31. Kraszewski K, et al. (1995) Synaptic vesicle dynamics in living cultured hippocampal neurons visualized with CY3-conjugated antibodies directed against the lumenal domain of synaptotagmin. *J Neurosci* 15:4328–4342.
32. Malgaroli A, et al. (1995) Presynaptic component of long-term potentiation visualized at individual hippocampal synapses. *Science* 268:1624–1628.
33. Atasoy D, et al. (2008) Spontaneous and evoked glutamate release activates two populations of NMDA receptors with limited overlap. *J Neurosci* 28:10151–10166.
34. Clements JD, Bekkers JM (1997) Detection of spontaneous synaptic events with an optimally scaled template. *Biophys J* 73:220–229.
35. Jakawich SJ, et al. (2010) Local presynaptic activity gates retrograde homeostatic changes in presynaptic function driven by dendritic BDNF synthesis. *Neuron*, in press.
36. Sara Y, Virmani T, Deák F, Liu X, Kavalali ET (2005) An isolated pool of vesicles recycles at rest and drives spontaneous neurotransmission. *Neuron* 45:563–573.
37. Fredj NB, Burrone J (2009) A resting pool of vesicles is responsible for spontaneous vesicle fusion at the synapse. *Nat Neurosci* 12:751–758.
38. Voglmaier SM, et al. (2006) Distinct endocytic pathways control the rate and extent of synaptic vesicle protein recycling. *Neuron* 51:71–84.
39. Chen G, Kolbeck R, Barde YA, Bonhoeffer T, Kossel A (1999) Relative contribution of endogenous neurotrophins in hippocampal long-term potentiation. *J Neurosci* 19:7983–7990.
40. Akaike T, et al. (1993) Antagonistic action of imidazolineoxyl N-oxides against endothelium-derived relaxing factor/.NO through a radical reaction. *Biochemistry* 32:827–832.
41. Bergquist S, Dickman DK, Davis GW (2010) A hierarchy of cell intrinsic and target-derived homeostatic signaling. *Neuron* 66:220–234.
42. Lessmann V, Heumann R (1998) Modulation of unitary glutamatergic synapses by neurotrophin-4/5 or brain-derived neurotrophic factor in hippocampal microcultures: Presynaptic enhancement depends on pre-established paired-pulse facilitation. *Neuroscience* 86:399–413.
43. Li Y-X, et al. (1998) Expression of a dominant negative TrkB receptor, T1, reveals a requirement for presynaptic signaling in BDNF-induced synaptic potentiation in cultured hippocampal neurons. *Proc Natl Acad Sci USA* 95:10884–10889.
44. Serulle Y, et al. (2007) A GluR1-cGKII interaction regulates AMPA receptor trafficking. *Neuron* 56:670–688.
45. Sejnowski TJ (1977) Storing covariance with nonlinearly interacting neurons. *J Math Biol* 4:303–321.
46. Koester HJ, Johnston D (2005) Target cell-dependent normalization of transmitter release at neocortical synapses. *Science* 308:863–866.
47. Hardingham NR, et al. (2010) Quantal analysis reveals a functional correlation between presynaptic and postsynaptic efficacy in excitatory connections from rat neocortex. *J Neurosci* 30:1441–1451.
48. Wheeler DG, Cooper E (2004) Weak synaptic activity induces ongoing signaling to the nucleus that is enhanced by BDNF and suppressed by low-levels of nicotine. *Mol Cell Neurosci* 26:50–62.
49. Ehlers MD, Heine M, Groc L, Lee M-C, Choquet D (2007) Diffusional trapping of GluR1 AMPA receptors by input-specific synaptic activity. *Neuron* 54:447–460.
50. Deisseroth K, Bito H, Tsien RW (1996) Signaling from synapse to nucleus: Postsynaptic CREB phosphorylation during multiple forms of hippocampal synaptic plasticity. *Neuron* 16:89–101.

NEUROSCIENCE